Characteristics of a polymer Mach-Zehnder electro-optic switch using side-coupled series-cascaded *M* microrings*

LI Cui-ting (李翠婷), **ZHENG Li-hua** (郑力华), **ZHENG Yue** (郑悦), **LI Chuan-nan** (李传南), **and ZHENG Chuan-tao** (郑传涛)**

State Key Laboratory on Integrated Optoelectronics, College of Electronic Science and Engineering, Jilin University, Changchun 130012, China

(Received 31 January 2015)

Structure and design are proposed for a kind of novel polymer Mach-Zehnder electro-optic (EO) switch using side-coupled *M* series-cascaded EO microrings. Formulations are proposed to analyze its switching characteristics. The dependences of the device's performances on *M* are thoroughly analyzed and concluded. As the increase of *M* from 2 to 10, the switching voltages for the 9 devices are as low as 0.84 V, 0.82 V, 0.52 V, 0.5 V, 0.37 V, 0.36 V, 0.29 V, 0.28 V and 0.24 V, respectively; whereas the crosstalks under bar state are within −20.79-−6.53 dB and those under cross state are within −20.36-−5.29 dB. The analysis results indicate that a smaller *M* is preferred for dropping the insertion loss and crosstalk, and a larger *M* should be selected to increase the optical bandwidth and minimize the switching energy. Generally, due to low switching voltage, the proposed device shows potential applications in optical networks-on-chip.

Document code: A **Article ID:** 1673-1905(2015)03-0179-5

DOI 10.1007/s11801-015-5022-1

Polymer optical switches based on linear electro-optic (EO) effect[1,2] have wide applications in optical communication systems, optical sensing systems, etc. In the past few years, different kinds of polymer EO switches have been numerically proposed by our group since 2008. Generally, there are three kinds described as below. The first kind is based on directional coupler (DC) structure[1,3,4], such as standard DC and Y-fed DC. Besides DC, Mach-Zehnder interferometer (MZI) is a simple but preferred structure used in optical switches[5,6]. Usually, an MZI switch should be incorporated with other structures, such as DC-assisted MZI and phase-generating coupler (PGC) assisted MZI. Due to small dimensions, ring resonator based devices can be densely integrated onto optoelectronic chips[7,8]. Therefore, the third kind of EO switch reported by our group is based on microring resonator (MRR) structure, such as the grid-type routing switch matrix based on two-ring cross-coupling resonators[9]. As a difference from the above switching configurations, combining the advantages of interference effect of MZI and phase-tuning effect of MRR, a kind of novel EO switch using side-coupled series-cascaded *M* microrings is proposed, where one group *M*-serial-oupled EO micorings are side-coupled with one arm of the MZI.

The structural model of the polymer MZI EO switch is shown in Fig.1(a). This device consists of input/output waveguides, two passive DCs serving as mode splitter and mode combiner, eight arc-transitive bending waveguides, and two MZI arms. One arm couples with one group of *M*-serial-coupled EO microrings (with identical radius r), and the other one is a passive waveguide. The coupling region lengths of the optical splitter and optical combiner are both L_1, and the bending radius of the arc-transitive waveguide is R. An extending waveguide with a length of L_2 is used to couple with the MRR waveguide. For the 3-dB DC, the gap between two coupling waveguides is d. The coupling gap between the upper MZI waveguide and the MRR waveguide is h_{CR}, and that between two adjacent microrings is h_{RR}. The length of the phase-shifter is $L_{pha} = 2L_2$.

The cross-section view AA' between an MRR waveide and the upper MZI waveguide is shown in Fig.1(b). The electrode is only deposited on microrings, for static operation, the applied direct-current voltage is U, and for dynamic operation, the applied time-dependent signal is $u_g(t)$. The MRR waveguide layers are: upper confined layer/upper electrode/upper buffer layer/EO core layer/ nder buffer layer/under electrode/Si substrate. Let t_1, t_2 and t_3 be the thicknesses of the core, buffer layer and electrode, respectively, and let w_r be the width of the rectangular

* This work has been supported by the National Natural Science Foundation of China (Nos.61107021, 61177027 and 61077074), the Ministry of Education of China (Nos.20110061120052 and 20120061130008), and the Science and Technology Department of Jilin Province of China (No.20130522161JH).

** E-mail: zhengchuantao578@163.com

waveguide. For the passive waveguide, the under buffer layer thickness is t_2+t_3. Because of bending, the core width of the MRR waveguide is slightly different from that of the channel waveguide (defined as w_c) for obtaining index-match between the two waveguides (U=0 V).

Under 1 550 nm, relative material parameters are taken as: the refractive index of the EO polymer material (AJL8/APC) is n_{10} =1.59, its bulk amplitude attenuation coefficient is α_{10} =0.25 dB/cm, and its EO coefficient is γ_{33}=68 pm/V[10,11]; the refractive index of the upper/under buffer layer material [P(PFS-GMA)] is n_{20} =1.461, and its bulk amplitude attenuation coefficient is α_{20} =0.25 dB/cm[12]; the electrode is made of aurum, its refractive index is n_{30} =0.19, and its bulk extinction coefficient is κ_{30}=6.1[13].

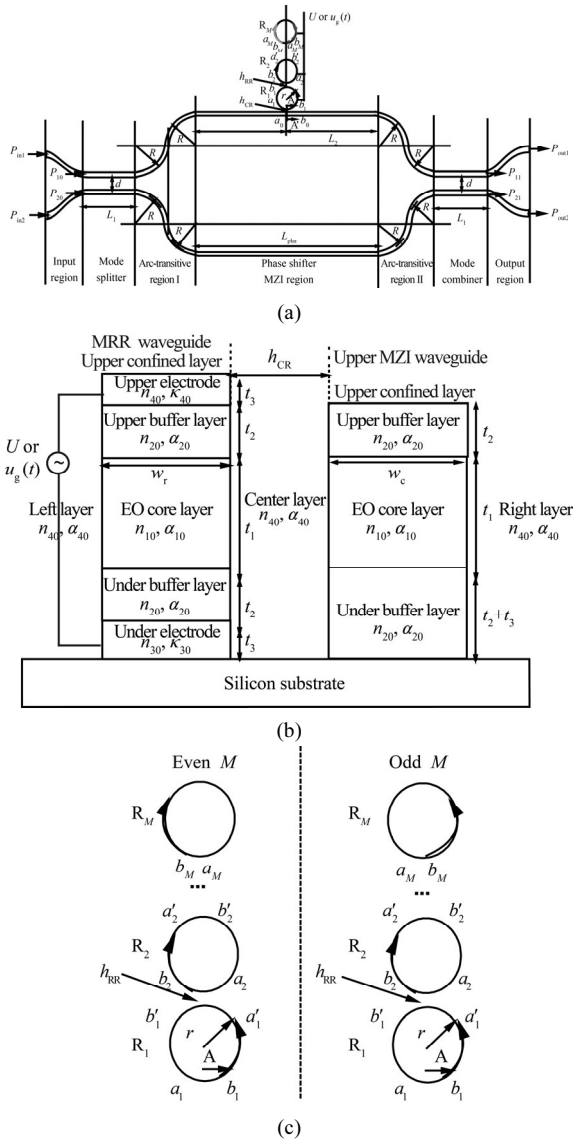

Fig.1 (a) Structural model of the polymer MZI EO switch/filter using an MZI and a side-coupled microring array; (b) Waveguide cross-section AA' between an active MRR waveguide and the upper passive MZI waveguide; (c) Structure of the series-cascaded *M* microrings

According to EO modulation theory, the variation of refractive index Δn_{10} of the EO core material of MRR waveguide versus U is

$$\Delta n_{10}(U)=\frac{1}{2}n_{10}^3\gamma_{33}E=\frac{n_{10}^3n_{20}^2\gamma_{33}U}{2(2n_{10}^2t_2+n_{20}^2t_1)}, \tag{1}$$

where U can be equal to zero or not. The refractive index of the EO core material n_{10} will be changed to n_{10}+Δn_{10}. Then the mode propagation constant in the active waveguide can be regarded as a function of U, denoted by $\beta_R(U)$, and accordingly, the optical mode loss can be denoted by $\alpha_R(U)$.

For the M-serial-coupled microring resonator, under an even and odd M, the resonator structure and its light propagation direction are shown in Fig.1(c). For microring R_j, let a_j and b_j (j =1, 2, ... M) be the light amplitudes of the lower coupling point, and a'_j and b'_j (j =1, 2, ... M-1) be those of the upper coupling point, which can be seen from Fig.1(c). Define κ_j and t_j (j =1, 2, ... M-1) as the amplitude coupling ratio and amplitude transmission ratio between R_j and R_{j+1}, respectively, and they satisfy the relation of $\kappa_j^2+t_j^2=1$. Define κ_{CR} and t_{CR} as the amplitude coupling ratio and amplitude transmission ratio between R_1 and the upper MZI arm, respectively, which satisfy the relation of $\kappa_{CR}^2+t_{CR}^2=1$. Let a_0 and b_0 be the light amplitudes of the coupling point between R_1 and the upper MZI arm. Based on resonance theory and transfer matrix method, we can obtain

$$b_0=\frac{f_1-t_{CR}f_2}{t_{CR}f_1-f_2}a_0, \tag{2}$$

where $f_1=\dfrac{\boldsymbol{Q}_R^{M-1}(1,2)-\boldsymbol{Q}_R^{M-1}(2,2)\exp(-j\phi_{R2})}{\boldsymbol{Q}_R^{M-1}(2,1)\boldsymbol{Q}_R^{M-1}(1,2)-\boldsymbol{Q}_R^{M-1}(1,1)\boldsymbol{Q}_R^{M-1}(2,2)}$,

$f_2=\dfrac{\boldsymbol{Q}_R^{M-1}(2,1)\exp(-j\phi_{R2})-\boldsymbol{Q}_R^{M-1}(1,1)}{\boldsymbol{Q}_R^{M-1}(2,1)\boldsymbol{Q}_R^{M-1}(1,2)-\boldsymbol{Q}_R^{M-1}(1,1)\boldsymbol{Q}_R^{M-1}(2,2)}$, $\phi_{R2}=2\pi r\cdot(\beta_R-j\alpha_R)$, and $\boldsymbol{Q}_R=\dfrac{1}{j\kappa_j}\begin{bmatrix}-\exp(j\phi_j) & t_j\exp(-j\phi_j)\\ -t_j\exp(j\phi_j) & \exp(-j\phi_j)\end{bmatrix}$.

Then the transfer function of the upper MZI arm can be expressed as

$$T_{upp}=\left[\frac{f_1-t_{CR}f_2}{t_{CR}f_1-f_2}\right]\exp\left[-j2(\beta_{c0}-j\alpha_{c0})L_2\right], \tag{3}$$

where β_{c0} and α_{c0} are mode propagation constant and amplitude loss coefficient of the passive straight MZI waveguide, respectively.

For the splitter and combiner, define φ_d as the angular coupling coefficient. Then the amplitude transfer matrix of the splitter and that of the combiner can both be written as

$$\boldsymbol{T}_{DC,1}=\boldsymbol{T}_{DC,2}=\exp(-\alpha_{c0}L_1)\begin{pmatrix}\cos\varphi_d & -j\sin\varphi_d\\ -j\sin\varphi_d & \cos\varphi_d\end{pmatrix}. \tag{4}$$

The transfer function of the lower passive MZI arm is

$$T_{\text{und}} = \exp\left[-\mathrm{j}\left(\beta_{\text{C0}} - \mathrm{j}\alpha_{\text{C0}}\right)L_{\text{pha}}\right]. \quad (5)$$

Let the light with an original amplitude of A_0=R_0 input into the upper waveguide only, namely, $P_{10} = P_0 = \left|A_0\right|^2 = \left|R_0\right|^2$ and $P_{20} = \left|B_0\right|^2 = 0$. Combining Eqs.(2)-(5), we can obtain the output power as

$$P_{\text{out1}}^{\text{in1}}(\text{dB}) = 10\lg\left|A\right|/R_0\Big|^2,\ P_{\text{out2}}^{\text{in1}}(\text{dB}) = 10\lg\left|B\right|/R_0\Big|^2, \quad (6)$$

with

$$A\big|_{\text{in1}} = R_0\exp\left(-2\alpha_{\text{c0}}L_1\right)\exp\left(-\mathrm{j}4\Psi_{\text{arc1}}\right)\cdot$$
$$\left\{\left[\frac{f_1 - t_{\text{CR}}f_2}{t_{\text{CR}}f_1 - f_2}\right]\exp\left[-\mathrm{j}2\left(\beta_{\text{c0}} - \mathrm{j}\alpha_{\text{c0}}\right)L_2\right]\left(\cos\varphi_{\text{d}}\right)^2 -\right.$$
$$\left.\exp\left[-\mathrm{j}\left(\beta_{\text{C0}} - \mathrm{j}\alpha_{\text{C0}}\right)L_{\text{pha}}\right]\left(\sin\varphi_{\text{d}}\right)^2\right\}, \quad (7)$$

$$B\big|_{\text{in1}} = -\mathrm{j}R_0\sin\varphi_{\text{d}}\cos\varphi_{\text{d}}\exp\left(-2\alpha_{\text{c0}}L_1\right)\exp\left(-\mathrm{j}4\Psi_{\text{arc1}}\right)\cdot$$
$$\left\{\left[\frac{f_1 - t_{\text{CR}}f_2}{t_{\text{CR}}f_1 - f_2}\right]\exp\left[-\mathrm{j}2\left(\beta_{\text{c0}} - \mathrm{j}\alpha_{\text{c0}}\right)L_2\right] +\right.$$
$$\left.\exp\left[-\mathrm{j}\left(\beta_{\text{C0}} - \mathrm{j}\alpha_{\text{C0}}\right)L_{\text{pha}}\right]\right\}, \quad (8)$$

$$\Psi_{\text{arc1}} = \left(\pi R/2\right)\left(\beta_{\text{arc1}} - \mathrm{j}\alpha_{\text{arc1}}\right), \quad (9)$$

where β_{arc1} and α_{arc1} are the mode propagation constant and mode amplitude loss coefficient, respectively.

By using our presented analysis theory in Refs.[5,14], the waveguide parameters are optimized at 1 550 nm wavelength, which are listed in Tab.1.

Tab.1 Optimized parameters of the switch

Parameter	Optimized value	Parameter	Optimized value
r	19.49 μm	n_4	1.0
Core thickness t_1	1.7 μm	α_4	0
Core width w_{c}	1.85 μm	R	40 μm
Core width w_{r}	1.7 μm	L_2, L_3	20 μm
Buffer thickness t_2	2.5 μm	Ring waveguide mode effective index n_{R}	1.518 9
Resonance order m	120	waveguide mode loss coefficient α_{C}, α_{R}	0.256 dB/cm
Coupling gap d	0.8 μm	h_{CR}	0.14 μm
Electrode thickness b_3	0.2 μm	h_{RR}	0.68 μm
Coupling length L_0	1 547.88 μm	Amplitude coupling ratio κ_{RR}	6.85×10^{-3}
Coupling region length L_1	773.94 μm	Amplitude coupling ratio κ_{CR}	1.25×10^{-1}

Based on Eq.(6), the relations between the output powers from the devices with different M and U are investigated, as shown in Figs.2(a)-(d). Fig.2(e) shows the curves of P_{out2}−P_{out1} versus U. One can observe from Fig.2(e) that though the devices with even M (cross state) and those with odd M (bar state) are under different operation states at U=0 V (the reason can be attributed to difference between the phase-shift resulting from odd-number of rings and that from even-number of rings when U is not sufficiently large), the curves will finally turn out to be the same operation state (e.g. cross-state) as U gets sufficiently large, as also proven by Figs.2(a)-(d). As the increase of M from 2 to 10, the switching voltages for the 9 devices are 0.84 V, 0.82 V, 0.52 V, 0.5 V, 0.37 V, 0.36 V, 0.29 V, 0.28 V and 0.24 V, respectively; whereas the crosstalks under bar state are within −20.79-−6.53 dB and those under cross state are within −20.36-−5.29 dB.

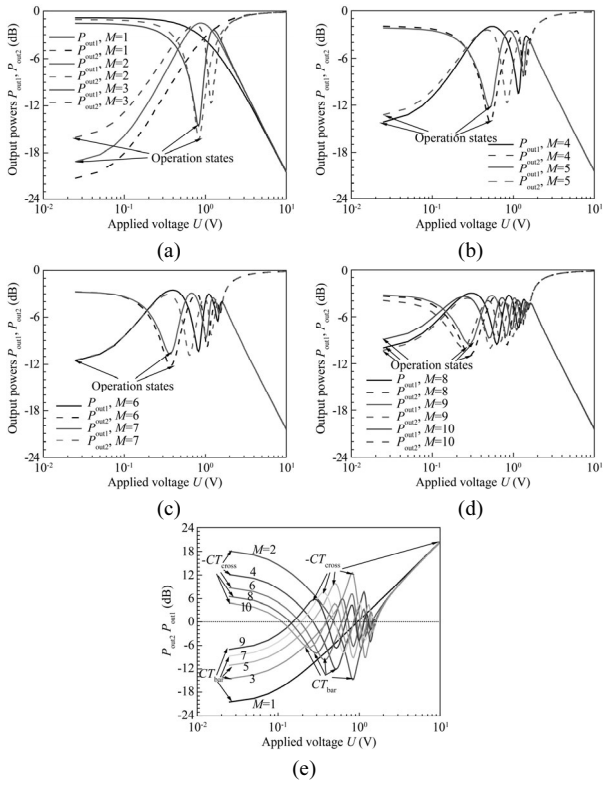

Fig.2 Curves of the output powers P_{out1} and P_{out2} versus the applied voltage U under 1 550 nm wavelength, where the light is input into the upper port only: (a) M = 1, 2, 3, (b) M = 4, 5, (c) M = 6, 7, (d) M = 8, 9, 10; (e) Curves of P_{out2}–P_{out1} versus U for the MZI EO switches

For the 3 devices with M=1, 3, 5, Fig.3 shows the spectral responses under both operation states. The results in Figs.3(a)-(c) indicate that the 3 switches perform good switching functions at 1 550 nm wavelength under the corresponding two applied voltages. Except for the situation of M=1, under the selection of operation states for each switch, we can notice the effects of M on the spectrum property, crosstalk and driving voltage. Furthermore, we can also conclude that the EO switch will experience 2M exchanges between the two output pow-

ers. For example, when M=1, the curve of $P_{out2}-P_{out1}$ firstly decreases and then increases, and two exchanges are found between P_{out2} and P_{out1}.

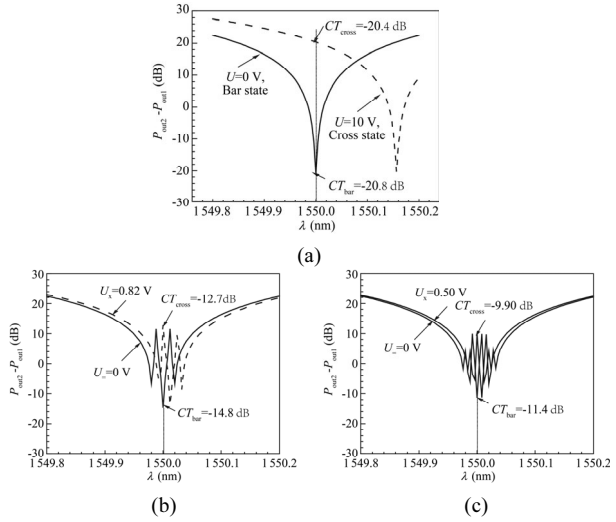

Fig.3 Spectral responses of the EO switches under both operation states: (a) *M*=1; (b) *M*=3; (c) *M*=5

Since the switch is driven in lumped manner, under the operation of a square-wave switching signal (e.g. U=$u_g(t)$), the electrical response can be calculated by

$$u_e(f,t)=F^{-1}\left[U_g(\omega)H(\omega)\right], \tag{10}$$

where $U_g(\omega)$=$F\left[u_g(t)\right]$ is the Fourier transformation of the applied square-wave signal, $H(\omega)=\left(1+\mathrm{j}\omega R_g C_e\right)^{-1}$ is the transfer function of the equivalent driving circuit, C_e is an equivalent capacitance including the electrode capacitance and the distributed capacitance, and R_g=50 Ω is the output resistance of the driving source. The time-dependent optical responses in non-dB form can be expressed as

$$P_{out1}^{in1}(f,t)=\left|A\right|_{in1}\left[u_e(f,t)\right]\Big|^2,$$

$$P_{out2}^{in1}(f,t)=\left|B\right|_{in1}\left[u_e(f,t)\right]\Big|^2. \tag{11}$$

Using Eq.(11), under the operation of a square-wave signal ($|U_×-U_=|$/2-V_{pp}, ($U_×$+$U_=$)/2-V_{bias}, f-frequency), the normalized optical response amplitudes and electrical response amplitude versus switching frequency are shown in Figs.4(a)-(c), where the capacitance of each microring electrode is calculated to be 6.11×10^{-4} pF, and the distributed capacitance is assumed to be 10 times of the capacitance of each microring electrode. It can be found from Figs.4(a)-(c) that the increase of M will lead to the decrease in optical bandwidth because of the increase of distributed capacitance, and the increase of M will slightly increase the electrical bandwidth (at least in trend).

The dynamic switching power of the device can be evaluated by the power consumption of the output resistance of the driving source, which is expressed as

$$PC(f)=f\int_T\frac{1}{R_g}\left[u_g(t)-u_e(t)\right]^2\mathrm{d}t, \tag{12}$$

where T=1/f is the period of the switching signal. The switching energy per bit can be calculated by

$$Q=PC(f)/f=\int_T\frac{1}{R_g}\left[u_g(t)-u_e(t)\right]^2\mathrm{d}t. \tag{13}$$

With Eq.(12), the influence of M on the switching power is shown in Fig.4(d). One can observe that the increase of M will drop the power consumption (e.g. from 63.2 mW under M=1 to 0.08 mW under M=9, at 10 GHz).

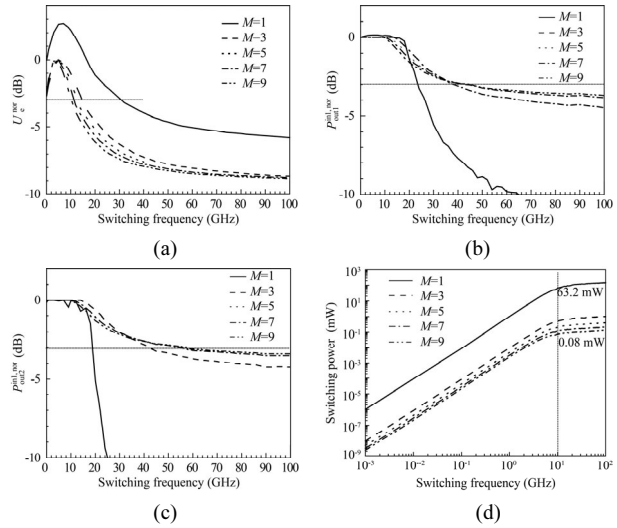

Fig.4 (a) The normalized electrical response amplitude and (b, c) optical response amplitudes of the five switches (*M*=1, 3, 5, 7, 9) under the operation of a square-wave signal ($|U_×-U_=|$/2-V_{pp}, ($U_×$+$U_=$)/2-V_{bias}); (d) Curves of switching power versus switching frequency *f* of the five switches (*M*=1, 3, 5, 7, 9)

As a conclusion, a kind of novel MZI EO switch is proposed, where M-serial-coupled EO micorings are side-coupled with one arm of MZI. Using the derived formulas and expressions, design, optimization and simulation are performed. The insertion losses and crosstalks at both operation states almost show the same trend as M changes, and a smaller M is preferred for dropping the insertion loss and crosstalk. However, in order to increase the optical bandwidth and minimize the switching energy, M should be selected as large as possible. The proposed multifunctional device shows potential applications in optical networks-on-chip.

References

[1] C.T. Zheng, Q.Q. Luo, L. Liang, C.S. Ma and D.M. Zhang, IEEE Journal of Quantum Electron **49**, 652 (2013).

[2] Y. Enami, D. Mathine, C.T. DeRose, R.A. Norwood, J. Luo, A.K.Y. Jen and N. Peyghambarian, Applied Physics Letters **94**, 213513 (2009).

[3] C.T. Zheng, C.S. Ma, X. Yan, X.Y. Wang and D.M. Zhang, Applied Physics B-Lasers and Optics **96**, 95 (2009).

[4] C.T. Zheng, C.S. Ma, X. Yan, X.Y. Wang and D.M. Zhang, Applied Physics B-Lasers and Optics **98**, 511 (2010).

[5] C.T. Zheng, C.S. Ma, X. Yan, X.Y. Wang and D.M. Zhang, Optics and Laser Technology **42**, 457 (2010).

[6] C.T. Zheng, C.S. Ma, X. Yan and D.M. Zhang, Applied Physics B-Lasers and Optics **102**, 831 (2011).

[7] K. Takahashi, Y. Kanamori, Y. Kokubun and K. Hane, Optics Express **16**, 14421 (2008).

[8] H. Simos, A. Bogris, N. Raptis and D. Syvridis, IEEE Photonics Technology Letters **22**, 206 (2010).

[9] C.T. Zheng, L. Liang, Q.Q. Luo, C.S. Ma, D.M. Zhang and Y.D. Wang, IEEE Photonics Journal **5**, 7200620 (2013).

[10] G.Y. Xu, Z.F. Liu, J. Ma, B.Y. Liu, S.T. Ho, L. Wang, P.W. Zhu, T.J. Marks, J.D. Luo and A.K.Y. Jen, Optics Express **13**, 7380 (2005).

[11] J. Luo, S. Liu, M. Haller, J. Kang, T. Kim, S. Jang, B. Chen, N. Tucker, H. Li, H. Tang, L. Dalton, Y. Liao, B.H. Robinson and A.K-Y. Jen, Organic Photonic Materials and Devices VI **5351**, 36 (2004).

[12] C. Pitois, S. Vukmirovic, A. Hult, D. Wiesmann and M. Robertsson, Macromolecules **32**, 2903 (1999).

[13] W.G. Driscoll and W. Vaughan, Handbook of Optics, New York, USA: McGraw-Hill, 7 (1978).

[14] E.A.J. Marcatili, Bell System Technical Journal **48**, 2103 (1969).